Live-cell single-molecule labeling and analysis of myosin motors with quantum dots

Hiroyasu Hatakeyama[a,b,*], Yoshihito Nakahata[c], Hirokazu Yarimizu[c], and Makoto Kanzaki[b,c]
[a]Frontier Research Institute for Interdisciplinary Sciences, [b]Graduate School of Biomedical Engineering, and [c]Department of Information and Intelligent Systems, Tohoku University, Sendai 980-8579, Japan

ABSTRACT **Quantum dots (QDs) are a powerful tool for quantitatively analyzing dynamic cellular processes by single-particle tracking. However, tracking of intracellular molecules with QDs is limited by their inability to penetrate the plasma membrane and bind to specific molecules of interest. Although several techniques for overcoming these problems have been proposed, they are either complicated or inconvenient. To address this issue, in this study, we developed a simple, convenient, and nontoxic method for labeling intracellular molecules in cells using HaloTag technology and electroporation. We labeled intracellular myosin motors with this approach and tracked their movement within cells. By simultaneously imaging myosin movement and F-actin architecture, we observed that F-actin serves not only as a rail but also as a barrier for myosin movement. We analyzed the effect of insulin on the movement of several myosin motors, which have been suggested to regulate intracellular trafficking of the insulin-responsive glucose transporter GLUT4, but found no significant enhancement in myosin motor motility as a result of insulin treatment. Our approach expands the repertoire of proteins for which intracellular dynamics can be analyzed at the single-molecule level.**

Monitoring Editor
Gero Steinberg
University of Exeter

Received: Jun 14, 2016
Revised: Oct 28, 2016
Accepted: Nov 1, 2016

INTRODUCTION

Single-molecule imaging or single-particle tracking is a powerful approach for quantitatively analyzing dynamic cellular processes such as intracellular transport or membrane dynamics (Saxton, 2008; Chenouard *et al.*, 2014). Fluorescent semiconductor nanoparticle quantum dots (QDs) are a suitable tool for these approaches due to their extremely bright fluorescence and high photostability (Dahan *et al.*, 2003; Kairdolf *et al.*, 2013). However, two challenges associated with using QDs to track intracellular molecules in live cells are functionalization and internalization (Pierobon and Cappello, 2012). The former refers to the coupling of QDs to molecules of interest, and the latter refers to the delivery of functionalized QDs to the cytoplasm. The issue of functionalization is relatively easy to resolve, as QDs with primary amines or carboxyl moieties that can be used for conjugation to other molecules are now commercially available, along with QDs coated with streptavidin or secondary antibodies.

Several methods of internalization have been proposed, such as induction of lipid/polymer-assisted endocytosis (Derfus *et al.*, 2004; Duan and Nie, 2007), use of cell-penetrating peptides (Suzuki *et al.*, 2013), and activation of pinocytosis via a transient osmotic shock (Nelson *et al.*, 2009; Pierobon *et al.*, 2009). However, these approaches have several drawbacks, including complicated protocols, low labeling efficiency, and cytotoxicity. Microinjection is a direct way to deliver materials or molecules into the cytoplasm and nucleus (Dubertret *et al.*, 2002) but cannot label many cells simultaneously and is both complicated and invasive. Electroporation has also been used to deliver QDs into the cytoplasm (Chen and Gerion, 2004; Derfus *et al.*, 2004; Keren *et al.*, 2009) but was previously not suitable for adherent cells because it required preparation of a cell suspension that disrupts subcellular architecture. Recently a microfluidic device for electroporation was developed and used to introduce QDs into adherent cells that maintained their attachment to a substrate (Sun *et al.*, 2014), but this approach required microchannel fabrication. We previously developed a noninvasive QD-labeling method using intrinsic endocytotic/recycling activities

This article was published online ahead of print in MBoC in Press (http://www.molbiolcell.org/cgi/doi/10.1091/mbc.E16-06-0413) on November 9, 2016.

*Address correspondence to: Hiroyasu Hatakeyama (hatake@tohoku.ac.jp).

Abbreviations used: DMSO, dimethyl sulfoxide; EMCCD, electron-multiplying charge-coupled device; MSD, mean-square displacement; PBS, phosphate-buffered saline; PEG, polyethylene glycol; QD, quantum dot; sCMOS, scientific complementary metal oxide semiconductor; TAE, Tris base/acetic acid/ethylenediaminetetraacetic acid.

of membrane-recycling proteins, including the insulin-responsive glucose transporter GLUT4 and transferrin receptor, for quantitative analysis of the intracellular trafficking properties of those proteins (Fujita *et al.*, 2010; Hatakeyama and Kanzaki, 2011, 2013a,b), but it was still not possible to label other intracellular proteins than membrane-recycling proteins using this approach. Therefore a simple, convenient, and noncytotoxic approach for labeling any intracellular protein with QDs is needed.

The actin-dependent myosin molecular motors constitute a large and diverse superfamily, which can be divided into many different classes (Foth *et al.*, 2006; Odronitz and Kollmar, 2007; Hartman and Spudich, 2012). All myosin motors can associate with filamentous actin (F-actin) tracks via a head region that can bind and hydrolyze ATP, and the motors undergo stepwise movement on their tracks by using the energy of ATP hydrolysis. Traditionally, the mechanistic properties of myosin motors have been extensively analyzed with various in vitro assays, including single-molecule microscopy, optical tweezers, and atomic force microscopy (Kodera and Ando, 2014). These experiments provided extensive details regarding the intrinsic activities of myosin motors, but the intracellular behavior of the motors could not be clarified by such in vitro assays. Recently the dynamics of myosin V in living cells was investigated by labeling the motors with QDs via osmolytic pinocytosis (Nelson *et al.*, 2009; Pierobon *et al.*, 2009). Using this technique, multiple characteristics of intracellular myosin V motility, such as step size and processivity, were successfully measured. However, this method requires purification of recombinant myosin protein, which is a time-consuming process, and it has limited flexibility in the selection of target proteins. Many myosin motors are known to regulate various cellular processes, including intracellular transport of various cargoes (Seabra and Coudrier, 2004), and myosin Ic, myosin II, and myosin V have been reported to be involved in intracellular trafficking of GLUT4 (Bose *et al.*, 2002; Steimle *et al.*, 2005; Yoshizaki *et al.*, 2007). Although insulin induces phosphorylation of these motors, it remains unclear whether and how insulin regulates the intracellular behavior of these myosin motors.

In the present study, we developed a simple technique that can easily label various types of cytosolic proteins with QDs using HaloTag technology, by which specific covalent bonds are formed between the HaloTag fusion protein and small ligands (Los *et al.*, 2008). The functionalized molecules can then be electroporated into adherent cells that maintain their attachment to a substrate. Using this approach, we tracked the intracellular movement of myosin motors and analyzed the effect of insulin on this movement.

RESULTS

Functionalization and internalization of QDs

We used HaloTag technology to functionalize QDs and electroporation to enable internalization of the functionalized QDs (Figure 1A). The succimidyl HaloTag ligand was conjugated to QDs in a one-step reaction using QDs modified with amine-derivatized polyethylene glycol (PEG). To evaluate whether the resultant HaloTag ligand–QD conjugates could bind to native HaloTag-fusion proteins, we analyzed conjugates mixed with cell lysates containing human HaloTag-14-3-3β/α proteins by agarose gel electrophoresis (So *et al.*, 2006). The theoretical isoelectric point of the HaloTag-14-3-3β/α proteins was 4.75 (as calculated by ExPASy); therefore the proteins had a negative charge in Tris base/acetic acid/ethylenediaminetetraacetic acid (TAE) buffer (pH 7.4). HaloTag ligand–QDs bound to HaloTag–14-3-3β/α proteins were identified by their more rapid movement on the gel relative to that of unbound HaloTag ligand–QDs. As expected, QDs with a higher abundance of HaloTag ligand showed greater mobility

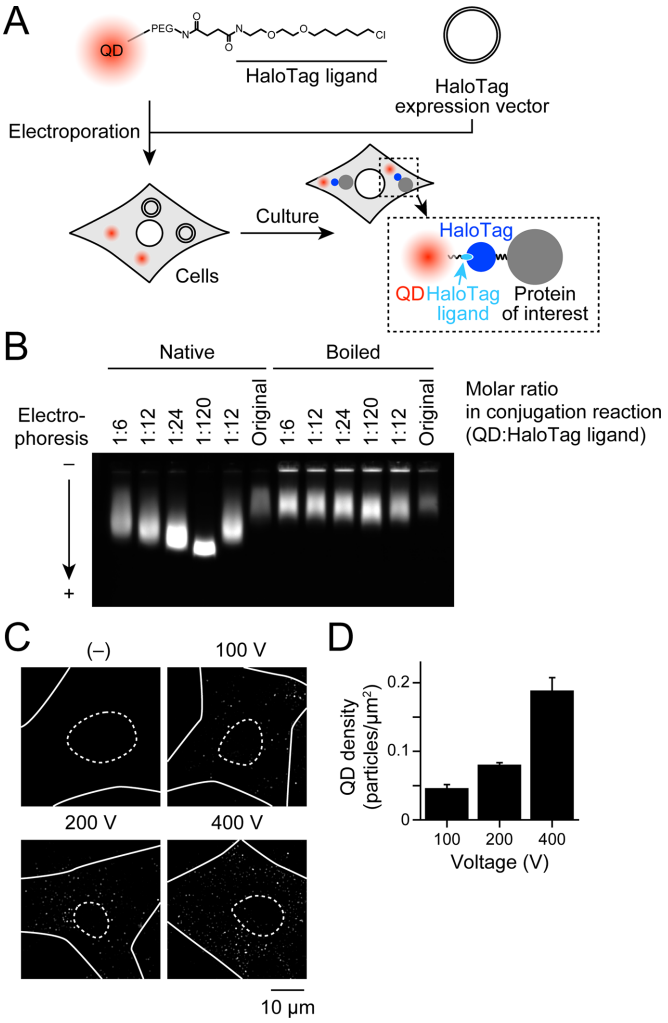

FIGURE 1: Approach for labeling intracellular proteins with QDs. (A) Schema for labeling intracellular proteins with QDs. (B) Binding of HaloTag ligand–QD with HaloTag proteins in vitro. HaloTag ligand–QDs were incubated with the lysate of KRX cells expressing HaloTag–14-3-3β/α proteins and separated on an agarose gel. Samples on the right half of the gel were denatured by boiling the lysates before mixing with HaloTag ligand–QDs. "Original" refers to QDs with no conjugation reaction. (C) Snapshots of QD fluorescence in 3T3-L1 fibroblasts. Cells were immersed with QD-containing solution, and electroporation was performed with the indicated poration pulse voltages. Solid and dashed lines represent plasma and nuclear membranes, respectively. The Laplacian of Gaussian-filtered images. (D) Dependence of internalization of QD in 3T3-L1 fibroblasts on poration pulse voltage.

(Figure 1B), which was not observed when mixing HaloTag ligand–QDs with HaloTag–14-3-3β/α protein samples that were denatured by boiling (Figure 1B).

Electroporation is an efficient means of inducing the uptake of QDs by cells (Chen and Gerion, 2004; Derfus *et al.*, 2004; Keren *et al.*, 2009); however, it typically requires preparation of a cell suspension and has nonnegligible cytotoxicity. We therefore used an electroporator that can be used in cells attached to standard culture dishes. We successfully introduced HaloTag ligand–QDs into cells in a manner dependent on the voltage of the poration pulse, whereas simple incubation of cells in HaloTag ligand-QD–containing solution did not result in internalization (Figure 1, C and D). When we used a

poration pulse of 400 V, the cells took up too many QDs for precise tracking of the movement of individual particles, and many cells were detached from the substrate. Therefore we set the poration pulse voltage at 200 V as the optimal voltage. The fraction of the cells that took up sufficient QDs was ~20% on average by visual inspection. The electroporation efficiency appeared to depend on the distance of the cells from the electrodes, that is, the cells located near the electrodes had a tendency to incorporate much more QDs, and therefore the electroporation efficiency was heterogeneous, as with other transfection methods. We typically chose the cells that incorporated 50–150 QDs/cell to precisely track individual QDs. The cells that remained attached appeared to be healthy upon inspection with trypan blue staining on the day after electroporation.

Tracking of HaloTag–myosin proteins

To verify the applicability of our approach, we tracked the intracellular movement of myosin Vb, a processive motor protein, labeled with QDs. First, vectors expressing myosin Vb heavy chain with HaloTag fused to its N terminus as well as HaloTag ligand–QDs were electroporated into 3T3-L1 fibroblasts, and QD fluorescence was visualized on the next day. Imaging was performed in cells expressing HaloTag–myosin Vb at low levels, which was confirmed by labeling the proteins, which were presumably not labeled with HaloTag ligand–QDs, with a membrane-permeable HaloTag TMR ligand. The observed amount of QD signal was sufficient for intracellular tracking (Figure 2A). Although some QD signals showed linear movement (Figure 2, B and C), they represented only ~5% of the total. Most of the QDs were almost immobile, consistent with previous reports (Nelson *et al.*, 2009; Pierobon *et al.*, 2009). We also analyzed the movement of HaloTag ligand–QD electroporated into cells that had been transfected with HaloTag–myosin Vb on the preceding day and after a few hours of QD electroporation. We observed slightly increased numbers of mobile HaloTag–QDs, but they still comprised no more than 10% of the total QD signals.

We quantified QD movement according to the mean-square displacement (MSD) and instantaneous diffusion coefficient (Figure 2, D and E). The mean diffusion coefficient of the QDs in the cells was 0.017 ± 0.005 μm^2/s (n = 9 cells), which was similar to the value from a previous study (0.018 ± 0.007 μm^2/s; Pierobon *et al.*, 2009). Of importance, HaloTag ligand–QDs in cells without expression of HaloTag proteins exhibited mainly random behavior (Figure 2F), and movement was more restricted in cells expressing HaloTag-fusion proteins other than myosin (unpublished data), confirming that the tracked molecules were HaloTag–myosin Vb. There were no obvious differences in the movement of QDs according to the number of HaloTag ligands on the QD (Supplemental Figure S1), in agreement with a previous study (Nelson *et al.*, 2009). We used HaloTag ligand–QD conjugates that had been prepared with a 1:12 M ratio in the conjugation reaction. We also analyzed the movement of myosin Vb with HaloTag fused to the C-terminus and found it to be slightly restricted (see later discussion of Figure 5C). There are no reports of differences in motility depending on the location of the tag, but the C-terminus is critical for targeting of proteins to specific intracellular compartments and binding to regulatory proteins such as Rab GTPases (Catlett and Weisman, 1998; Seabra and Coudrier, 2004), and studies analyzing myosin dynamics typically used N-terminal (Tsakraklides *et al.*, 1999; Buss *et al.*, 2001; Snyder *et al.*, 2004; Vicente-Manzanares *et al.*, 2007; Sandquist and Means, 2008) rather than C-terminal (Beach *et al.*, 2014) tags. We therefore used myosin with a HaloTag fused to its N-terminus for analyses.

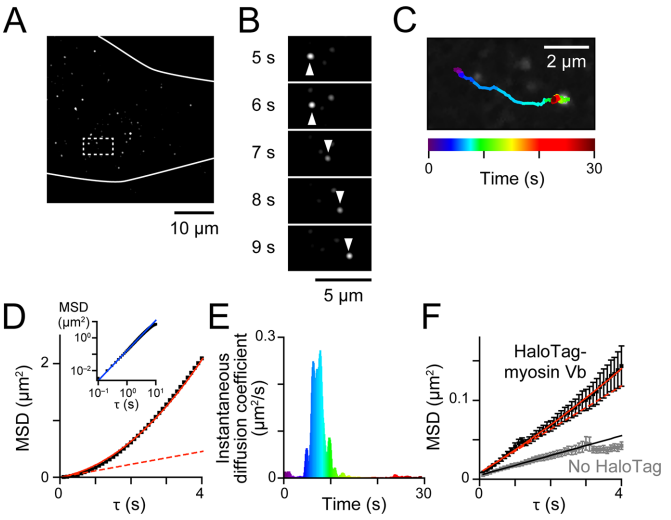

FIGURE 2: Tracking intracellular movement of HaloTag-myosin Vb. (A) QD fluorescence in a cell expressing HaloTag–myosin Vb labeled with HaloTag ligand–QDs. The Laplacian of Gaussian-filtered images. The solid line represents the plasma membrane. (B) Changes in the position of a labeled HaloTag–myosin Vb in the boxed region of A (arrowheads). (C) Trajectory of the particle shown in B. Color represents time as shown below the image. (D, E) MSD curve derived from the whole trajectory (D) and instantaneous diffusion coefficient (E) of the particle shown in B. Red solid and dashed lines in D are the best-fit curves with Eq. 2 and the linear component, respectively. The parameters are D = 0.028 μm^2/s and v = 0.32 μm/s. The blue solid line in the inset of D is the best-fit curve obtained using Eq. 4 with a value of 1.8 for exponent α, indicating that the movement was mainly dominated by directional movement. (F) Mean MSD curves of HaloTag ligand–QDs in cells expressing HaloTag–myosin Vb (black) or no HaloTag proteins (gray). The red solid and dashed lines are the best-fit curves obtained using Eq. 2 and the linear component, respectively. The parameters are D = 0.007 μm^2/s and v = 0.037 μm/s. The black solid line is the best-fit curve obtained using Eq. 3 with D = 0.003 μm^2/s. Data are presented as mean ± SEM.

We speculated that the QDs could be used to show linear movement of HaloTag–myosin Vb along F-actin. To determine whether this was indeed the case, we simultaneously visualized F-actin architecture by electroporating the expression vector Lifeact-Venus (Riedl *et al.*, 2008) along with HaloTag–myosin Vb and HaloTag ligand–QDs. Because QDs have a broad absorption spectrum and a large Stokes shift, it was possible to detect both fluorophores concurrently (Figure 3A). QDs were observed moving along thick F-actin tracks (Figure 3B), and the difference in angle between QD movement and F-actin was 1.5 ± 3.5° (mean ± SD, n = 10). Detailed analysis of the trajectories (Figure 3Ca) revealed that, as expected, the QDs largely dominated by directional movement (based on MSD curves shown in Figure 3Cb, particles i and ii) moved more rapidly on thick F-actin than those that were not on these filaments (Figure 3C, c and d), indicating that F-actin acts as a track for myosin Vb. Of interest, we occasionally observed that QDs mainly dominated by diffusion (particle iii) showed temporally slower movement when the QD was colocalized with F-actin (Figure 3Cc, asterisks). Such behavior may reflect that the myosin molecule searches for F-actin tracks during diffusional movement and, once the molecule finds F-actin, it may attempt to bind with the tracks, and the movement becomes slow. This observation suggests that the filaments may also act as a diffusional barrier for myosin movement.

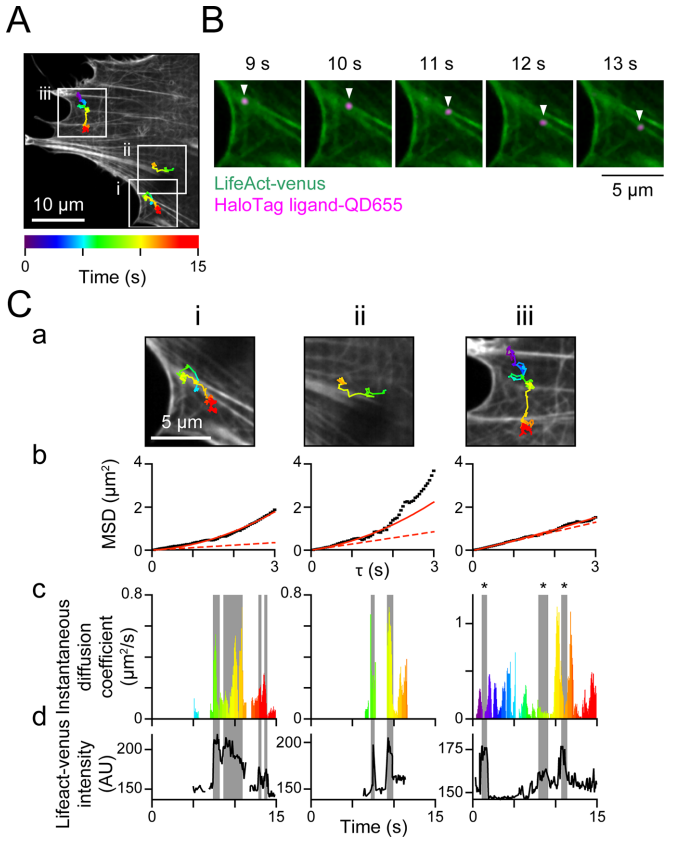

FIGURE 3: Simultaneous observation of HaloTag–myosin Vb and F-actin. (A) Lifeact-Venus fluorescence. Trajectories of three HaloTag–myosin Vb labeled particles with HaloTag ligand–QDs are overlaid. Colors represent time as shown below the image. (B) Changes in the position of a HaloTag ligand–QD signal (magenta) along Lifeact-Venus–labeled F-actin (green) in the boxed region (i) in A. The Laplacian of Gaussian-filtered QD images is shown. (C) Magnified images overlaid with trajectories (a), MSD curves (b), instantaneous diffusion coefficients (c), and Lifeact-Venus intensities (d) of the three particles shown in A. The solid and dashed lines in (b) are the best-fit curves and linear components obtained using Eq. 2, respectively. The fitted parameters of particles i–iii are, respectively, $D = 0.029$, 0.071, and 0.11 and μm²/s and $v = 0.40$, 0.39, and 0.16 μm/s. Shaded areas in c and d represent QDs colocalized with Lifeact-Venus signals, which were estimated by the fluorescence intensity of Lifeact-Venus along the trajectories. Asterisks in c represent restricted movement of QDs on thick F-actin.

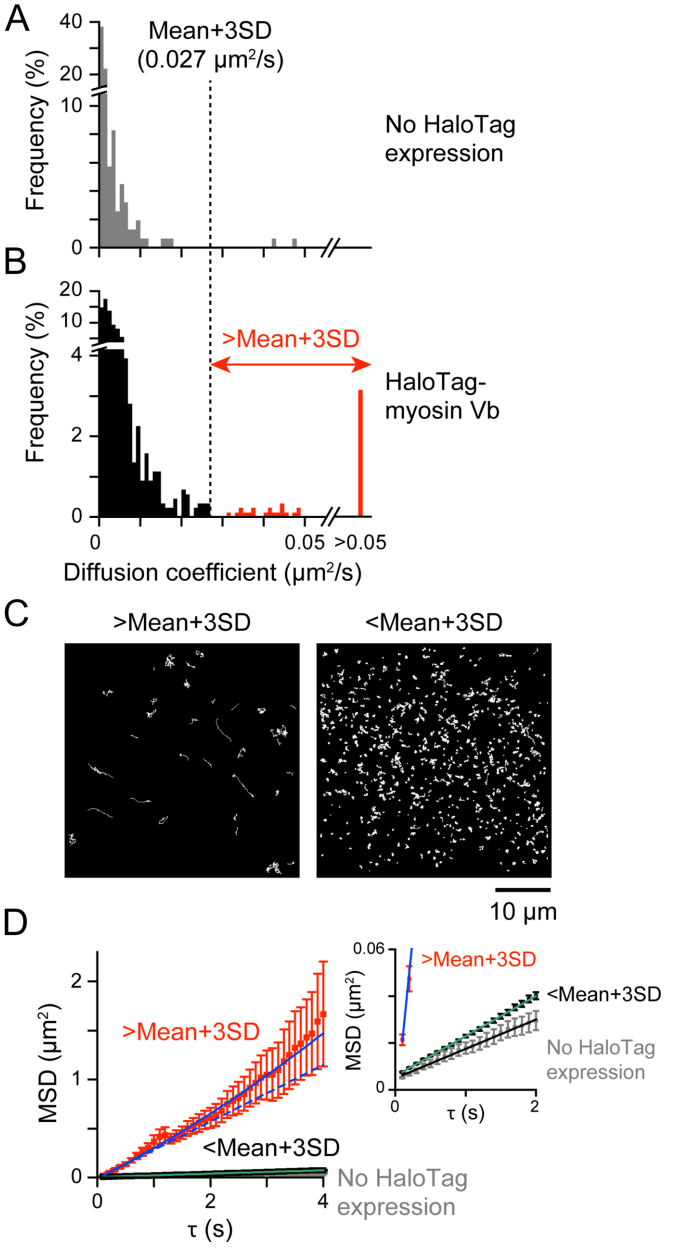

FIGURE 4: Analysis of fast-moving HaloTag–myosin molecules. (A, B) Histograms of diffusion coefficients of HaloTag ligand–QDs calculated from whole trajectories in cells expressing no HaloTag proteins (A) or HaloTag–myosin Vb (B). The dashed line represents the set threshold (diffusion coefficient of mean +3 SDs in A), and the red bars in B represent particles exceeding the threshold. Data were calculated from 157 particles in three cells in A and 891 particles in nine cells in B. In B, 48 of 891 particles (5.4%) exceeded the threshold. (C) Trajectories of HaloTag ligand–QD signals above (left) and below (right) the threshold. Overlaid trajectories obtained from nine cells. (D) MSD curves calculated from particles above (red) and below (black) the threshold. An MSD curve from cells expressing no HaloTag protein (gray) is shown for comparison. Right, magnified graph within $\tau < 2$ s and MSD < 0.06 μm². The MSD curve of particles exceeding and below the threshold was best-fitted with Eq. 2 with parameters of $D = 0.072$ and 0.004 μm²/s and $v = 0.14$ and 0.01 μm/s, respectively (blue and green solid lines). Data are presented as mean ± SEM.

Effect of insulin on myosin movement

We next investigated the effect of insulin on the movement of the nonprocessive myosins Ic and IIa and the processive myosin Vb, all of which are regulated by insulin and implicated in intracellular trafficking of GLUT4 (Bose *et al.*, 2002; Steimle *et al.*, 2005; Ishikura and Klip, 2008). However, the presence of many immobile QDs hindered single-particle tracking analysis of QD movement under various conditions. We therefore set a threshold of diffusion coefficients at >0.027 μm²/s to define mobile QDs, that is +3 SDs of the value for HaloTag ligand–QDs in cells without HaloTag protein expression (0.003 ± 0.008 μm²/s; Figure 4A). The fraction of QDs with a diffusion coefficient above the threshold was 5.4% in cells that underwent electroporation with both HaloTag ligand–QDs and

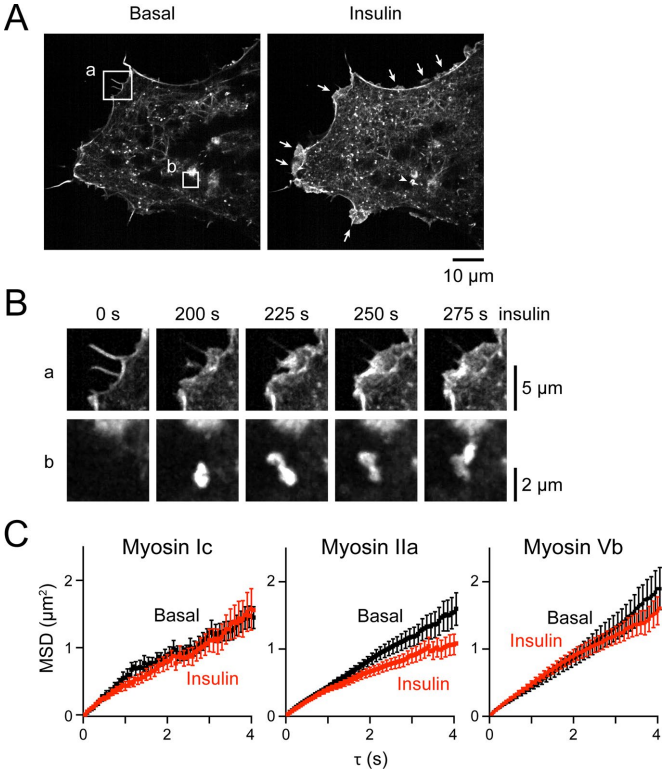

FIGURE 5: Effect of insulin on HaloTag–myosin movement. (A) Lifeact-Venus fluorescence before (left) and after 4 min of insulin stimulation (right) in 3T3-L1 fibroblasts. Membrane ruffling (arrows) and actin comet tails (arrowhead) were observed. Images are maximum intensity projections over five successive frames. (B) Magnified images of boxed regions shown in A. (C) MSD curves derived from the whole part of the trajectories having diffusion coefficients >0.027 μm²/s in cells expressing HaloTag-myosin Ic (left), HaloTag-myh9 (center), and HaloTag-myosin Vb (right) before (black) and 5 min after (red) insulin stimulation. Data are presented as mean ± SEM.

HaloTag–myosin Vb expression vectors simultaneously (mean diffusion coefficient, 0.18 ± 0.23 μm²/s; Figure 4B), or 7.5 and 6.5% after 3 and 6 h of electroporation into cells that had been transfected with HaloTag-myosin Vb on the preceding day, respectively. As expected, the trajectories of particles above the threshold were more linear (Figure 4C); thus their MSD curves had a more quadratic form than those of subthreshold particles (Figure 4D). Although the thresholding approach could potentially lead to inclusion of particles that do not show directional movement while omitting those that do, we deemed it suitable for effectively detecting mobile QDs.

We confirmed that insulin induced massive actin reorganization in 3T3-L1 fibroblasts, including membrane ruffling and formation of actin comet tails, within 5 min of stimulation, as visualized by Lifeact-Venus (Figure 5, A and B). We expressed myosin Ic, myosin IIa (myh9), and myosin Vb heavy chains with HaloTag fused to the N-terminus in 3T3-L1 fibroblasts and analyzed the movement of highly mobile (i.e., above the threshold) HaloTag ligand–QDs before and 5 min after insulin stimulation. There was a slight reduction in the movement of HaloTag-myh9 at longer (>2 s) but not shorter (<2 s) time delays in response to insulin (Figure 5C), suggesting that insulin reduced protein movement via secondary effects rather than by directly inhibiting the intrinsic motility of the motors. The other myosins examined here showed no significant changes in movement in the presence of insulin (Figure 5C).

DISCUSSION

We developed a simple and convenient method for labeling intracellular proteins with QDs using HaloTag technology to couple QDs to specific molecules of interest and electroporation to deliver the QDs to the cytosol. Although each of these techniques has already been separately applied to the analysis of dynamic cellular processes using QDs (Derfus *et al.*, 2004; So *et al.*, 2008; Liu *et al.*, 2012; Sun *et al.*, 2014), our approach enables the tracking of any cytosolic molecule that can be fused to the HaloTag and expressed in cells. Although Sun *et al.* (2014) also used electroporation to deliver QDs into the cytoplasm, our method has several advantages over their technique. The first and most important advantage is the use of HaloTag rather than an antibody. Obviously, the size of HaloTag proteins (33 kDa) is quite smaller than that of antibodies (150 kDa), and therefore the whole size of QD-labeled HaloTag protein complexes should be smaller than that of protein complexes labeled with QD-conjugated antibodies, which may enable tracking of proteins that undergo nuclear transport (Lowe *et al.*, 2010). In addition, by using HaloTag–QD conjugates with multiple HaloTag ligands on a single QD, it may be possible for multiple different functional proteins to be integrated around a QD as a core by expressing several HaloTag-fused proteins in the cells. Such an "artificial" complex could act as a local modulator of various cellular processes. Although the results are preliminary, we successfully generated such artificial complexes and modified the intracellular behavior of the proteins (unpublished data). In addition, our approach can increase flexibility in terms of the selection of molecules of interest once HaloTag ligand–QDs have been prepared, in contrast to labeling with antibodies that requires high specificity. The second advantage relates to the general usability of the methodology; we can perform electroporation into cells seeded in standard glass-bottom dishes rather than the special microfluidic devices used in the previous study (Sun *et al.*, 2014). Microfluidic devices have become popular recently, but special techniques, devices, and facilities for fabrication are still necessary and are not easily available. For cell biological studies, a critical aspect of QD electroporation into adherent cells that maintain their attachment to a substrate is that the QDs can be introduced onto cells without perturbing preexisting subcellular architecture, as various mature cellular functions are mediated by higher-ordered subcellular architectures. Some of this architecture is established during cellular differentiation (Kanzaki and Pessin, 2002; Fujita *et al.*, 2007) and is not maintained after the cells are detached. We also succeeded in QD electroporation into differentiated 3T3-L1 adipocytes (unpublished data).

Myosin V has traditionally been the focus of studies analyzing intracellular behavior using QDs (Nelson *et al.*, 2009; Pierobon *et al.*, 2009). In these studies, myosin V was functionalized by tagging the heavy meromyosin fragment with a biotin ligase recognition sequence (Nelson *et al.*, 2009) or by using biotinylated calmodulin light chain (Pierobon *et al.*, 2009). The biotinylated myosin was then purified and labeled with QDs by using streptavidin-QD in vitro before internalization into cells via osmolytic pinocytosis. Although our methods for functionalization and internalization were completely different, our results (e.g., the diffusion coefficient) were similar to those obtained in the aforementioned studies. Consistent with our present observations, the previous studies found that only a small fraction (~5%) of QDs showed linear movement. The small size of the mobile fraction may be attributed to several possibilities,

including 1) unconjugated QDs, 2) nonspecific binding of HaloTag ligand–QDs, and 3) binding of HaloTag ligand–QDs to inactive myosin motors. The first possibility is unlikely because our analysis with agarose gel electrophoresis revealed that almost all QDs that had undergone conjugation reactions appeared to be successfully coupled to HaloTag-fusion proteins (Figure 1C). Regarding the second possibility, the presence of many immobile HaloTag ligand–QDs in cells without expression of HaloTag-fusion proteins suggests that nonspecific binding inside the cells might have occurred. Although it is difficult to calculate the fraction of nonspecifically bound QDs, the fraction of active/mobile myosin molecules will be increased if this nonspecific binding is also included. Nevertheless, it is also important to note that all incorporated HaloTag ligand–QDs would be capable of binding with HaloTag-fusion proteins in the cells because the cells that were electroporated with both HaloTag ligand–QDs and HaloTag expression vectors can be further labeled with HaloTag TMR ligand. Therefore the number of HaloTag proteins expressed in the cells should be larger than that of HaloTag ligand–QDs incorporated into the cells. The third possibility introduces the exciting suggestion that such small fractions are sufficient for physiological cellular functions. This possibility can only be explored by single-molecule analysis, and further elucidation using various molecules, cells, or stimulations will be able to clearly explain why the mobile fractions are so small.

QDs are ideal for single-particle tracking but are not always appropriate for observing subcellular architecture because of the necessity of sparse labeling; fluorescent proteins are more suited to this purpose. Given that QDs have a broad absorption spectrum and a large Stokes shift, they can be concurrently visualized with other fluorescent molecules. In this study, we thus analyzed QD-labeled HaloTag–myosin movement along the Lifeact-Venus–labeled F-actin cytoskeleton by electroporating the QDs and the expression vectors concurrently (Figure 3). Of interest, we noted that some QDs showed transient restricted movement around thick F-actin, suggesting that the latter could act not only as a track but also as a diffusional barrier for movement of intracellular molecules including myosin. Such dual roles of F-actin have been suggested by other intracellular trafficking studies (Mathur *et al.*, 2003; Giner *et al.*, 2005, 2007). We cannot rule out the possibility that the observed HaloTag ligand–QDs have more than one HaloTag ligand per QD, in which case the restricted movement could reflect a tug-of-war between two or more F-actin filaments, and it may be possible to calculate rates of association/dissociation between myosin and F-actin by improving temporal resolution.

Many myosin motors, including both processive and nonprocessive types, are responsible for the intracellular transport of various cargoes (Seabra and Coudrier, 2004); some myosin motors are believed to regulate the trafficking of the insulin-responsive glucose transporter GLUT4. For example, the nonprocessive monomer myosin Ic has been reported to mediate GLUT4 translocation to the plasma membrane (Bose *et al.*, 2002, 2004) through binding with RalA small GTPase and the exocyst complex (Chen *et al.*, 2007). Insulin phosphorylates myosin Ic at Ser-701 via Ca^{2+}/calmodulin-dependent protein kinase II activity (Yip *et al.*, 2008). Nonprocessive nonmuscle myosin II, which is known to form homodimers via the α-helical coiled-coil region, regulates insulin-stimulated glucose uptake and fusion of GLUT4 vesicles to the plasma membrane (Steimle *et al.*, 2005; Fulcher *et al.*, 2008). Each myosin heavy chain of myosin II binds two distinct (i.e., essential and regulatory) calmodulin-like light chains, and insulin increases phosphorylation of the regulatory light chain of the protein (Choi *et al.*, 2006). The processive motors myosin Va and Vb, which also form homodimers, are also required for insulin-stimulated GLUT4 translocation (Yoshizaki *et al.*, 2007; Ishikura and Klip, 2008), and insulin increases phosphorylation of myosin Va at Ser-1650 via Akt (Yoshizaki *et al.*, 2007). Myosin motors are also known to regulate intracellular transport by acting as effectors of Rab small GTPases (Seabra and Coudrier, 2004; Miserey-Lenkei *et al.*, 2010), and insulin can modulate the activity of several Rab proteins (Sano *et al.*, 2003; Peck *et al.*, 2009). This suggests that insulin regulates a variety of myosin behaviors, including intrinsic motor activity or affinity to F-actin, that modulate GLUT4 trafficking in conjunction with Rab protein activity. In the present study, we expected that insulin would stimulate the intrinsic activity of myosin motors, but this was not the case (Figure 5C), although it did induce massive actin remodeling (Figure 5A). Nonetheless, insulin slightly decreased the movement of HaloTag-myh9, the heavy chain of myosin IIa. A characteristic feature of nonmuscle myosin II is its ability to assemble into bipolar minifilaments, which is regulated by its phosphorylation (Vicente-Manzanares *et al.*, 2007). Taken together with the previously observed fluorescence recovery after photobleaching measurements demonstrating that the turnover of phosphorylated myosin II is slower than that of the nonphosphorylated protein (Watanabe *et al.*, 2007a), the reduced movement after insulin stimulation observed here could reflect assembly/incorporation of myosin II into minifilaments. We also did not observe any obvious changes in the numbers or frequencies of HaloTag ligand–QDs on F-actin (unpublished data). Simultaneous imaging of GLUT4 and myosin in differentiated adipocytes is required to clarify the role of motors in GLUT4 trafficking; nonetheless, our observations suggest that actin remodeling rather than myosin motor activity itself regulates insulin-responsive GLUT4 trafficking (Kanzaki and Pessin, 2001; Kanzaki *et al.*, 2001). Insulin may regulate the activity of the other myosin motors examined in this study, as well as that of the microtubule-associated motors kinesin and dynein, which are also implicated in GLUT4 trafficking (Huang *et al.*, 2001; Imamura *et al.*, 2003; Semiz *et al.*, 2003). Our approach would be useful for analyzing the behavior of these molecules.

Several methodological issues need to be addressed. First, our approach acquires data as a time series of two-dimensional (2D) images, but in many instances, three-dimensional (3D) analyses are preferable—for example, when single-particle tracking is applied to higher-order samples such as tissues. Various methods for 3D tracking have been proposed, including postanalysis of acquired images (Holtzer *et al.*, 2007; Watanabe *et al.*, 2007b, 2013; Thompson *et al.*, 2010; Gardini *et al.*, 2015) and real-time 3D tracking (Ruthardt *et al.*, 2011; Liu *et al.*, 2013). Combining these techniques with our approach would provide further insight into dynamic cellular processes. The second issue is blinking, that is, the random switching between on and off states on a large time scale during continuous excitation, in QDs. This phenomenon can be almost completely eliminated by high concentrations of thiols such as mercaptoethanol or dithiothreitol (Hohng and Ha, 2004), but these agents are unsuitable for use in live cells. There have been numerous efforts to suppress QD blinking (Mahler *et al.*, 2008; Galland *et al.*, 2012; Chen *et al.*, 2013; Ji *et al.*, 2015), and novel materials without blinking have been developed, such as single-walled carbon nanotubes (Fakhri *et al.*, 2014). Our approach can be applied to materials other than QDs as long as they have functional groups that can be conjugated with HaloTag ligands. Furthermore, other protein tags, such as SNAP-tags, can be readily incorporated into our methodology. In summary, our simple and convenient method for labeling intracellular molecules with QDs is a valuable approach for investigating dynamic cellular processes at a single-molecule level.

MATERIALS AND METHODS

Plasmids

All HaloTag N-terminal mammalian expression vectors encoding HaloTag fused to myo1c (pFN21ASDB0033), myh9 (pFN21ASDB0014), myosin Vb (pFN21AA1119), and 14-3-3β/α (pFN21AB5474) were from Kazusa DNA Research Institute (Kisarazu, Japan). Cloning into C-terminal vectors (pFC14K vectors) was performed with the Carboxy Flexi System, Transfer (Promega, Madison, WI). The vectors encoding HaloTag-14-3-3β/α were transferred into bacterial expression vectors (pFN18K vectors) with Flexi System, Transfer. The Lifeact-Venus expression vector was provided by K. Ohashi (Tohoku University, Sendai, Japan).

HaloTag ligand–QD preparation and agarose gel electrophoresis

Conjugation of HaloTag ligand with QDs was performed using HaloTag succinimidyl ester (O2) ligand (Promega) and Qdot ITK amino (PEG) QD655 (Thermo Fisher Scientific, Waltham, MA). The Qdot storage buffer was replaced with phosphate-buffered saline (PBS; pH 7.4) after ultrafiltration and HaloTag succinimidyl ester ligand dissolved at 12 mM in anhydrous dimethyl sulfoxide (DMSO) was added. After a 30-min incubation at room temperature, unreacted ligand was removed by ultrafiltration. The HaloTag ligand–QD concentration was determined with the formula $A = \varepsilon cL$, where A, ε, c, and L are the absorbance at the specified wavelength, molar extinction coefficient, molar concentration, and path length, respectively. According to the manufacturer, ε has a value of 800,000 M^{-1} cm^{-1} at 638 nm. Conjugation reactions were performed at various QD:HaloTag ligand ratios (1:6 to 1:120).

HaloTag-14-3-3β/α proteins were expressed in KRX-competent cells (Promega) according to the manufacturer's instructions. In brief, the cells were grown until they reached an absorbance at 600 nm of 1.0–1.5 in Terrific Broth medium consisting of 1.2% Bacto-tryptone, 2.4% Bact-yeast extract, 0.4% glycerol, and 89 mM potassium phosphate. Protein expression was induced by addition of 0.1% rhamnose and 1 mM isopropyl β-D-1-thiogalactopyranoside at 17°C, and the cells were harvested after 16–24 h. The cell pellet was washed once with buffer consisting of 50 mM 4-(2-hydroxyethyl)-1-piperazineethanesulfonic acid (HEPES)–NaOH (pH 7.4), 150 mM NaCl, and 1 mM phenylmethylsulfonyl fluoride, and the cells were then resuspended in standard lysis buffer containing 1% Triton X-100, followed by sonication three times for 30 s each. The resultant lysate was divided into two parts, with one part boiled to denature the proteins; the lysates were then mixed with 50 nM HaloTag ligand–QDs for 1 h at 4°C and then analyzed by 0.5% agarose gel electrophoresis in 0.5× TAE buffer. QD fluorescence was detected with a Pharos FX Molecular Imager (Bio-Rad, Hercules, CA) at an excitation wavelength of 488 nm.

Cell culture and electroporation

3T3-L1 fibroblasts were seeded in glass-bottom dishes (thickness 0.17 mm; Matsunami Glass, Osaka, Japan) and cultured overnight in a humidified atmosphere of 5% CO_2/95% air at 37°C in DMEM supplemented with 10% calf serum. The cells were rinsed once with ice-cold PBS and then immersed in electroporation buffer consisting of 150 mM trehalose, 5 mM potassium phosphate buffer, 5 mM $MgCl_2$, 2 mM ethylene glycol tetraacetic acid, 2 mM ATP, 25 mM HEPES-KOH (pH 7.3), and 1% DMSO with 25 μg of plasmid DNA and 5 nM HaloTag ligand–QD. The imaging experiments other than those in Supplemental Figure S1 were performed with HaloTag ligand–QD prepared by 1:12 conjugation reactions. After a 3-min incubation on ice, electroporation was performed with a CUY21EDITII electroporator (BEX Co., Tokyo, Japan) and electrode (LF513-5; BEX Co.) by applying a poration pulse at 100–400 V for 10 ms, followed by five pulses at –30 V for 10 ms at 50-ms intervals. The cells were then washed and cultured overnight in the culture medium. In some experiments, the cells were first transfected with plasmid DNAs using Lipofectamine 3000 (Thermo Fisher Scientific) according to the manufacturer's instructions, and electroporation of HaloTag ligand–QDs was performed the next day.

Imaging and single-particle tracking

Fluorescence imaging was performed in cells immersed in imaging buffer consisting of 150 mM NaCl, 5 mM KCl, 2 mM $CaCl_2$, 1 mM $MgCl_2$, 10 mM HEPES-NaOH (pH 7.4), and 5.5 mM D-glucose at ~30°C using stage and lens heaters (TOKAI HIT, Fujinomiya, Japan) on an inverted microscope (IX81; Olympus, Tokyo, Japan) equipped with an electron-multiplying charge-coupled device (EMCCD) camera (iXon Ultra; Andor, Belfast, United Kingdom), a scientific complementary metal oxide semiconductor (sCMOS) camera (Zyla 4.2; Andor), a Nipkow disk confocal unit (CSU-X1; Yokogawa Electric Corporation, Tokyo, Japan), a two-camera imaging adapter (TuCam; Andor), and an oil-immersion objective lens (UPLSAPO100×O, numerical aperture 1.4; Olympus). QDs and Venus were both excited at 488 nm with a solid-state laser separated by a dichroic mirror with an edge wavelength of 560 nm (Semrock, Rochester, NY), and the signal was projected to the EMCCD and sCMOS cameras through 655/12 and 520/40 bandpass filters (Semrock), respectively. The two cameras and laser were synchronized, and images were acquired at 0.2–20 frames/s with an integration time of 50–100 ms/frame. Insulin was diluted to 100 nM in the imaging buffer and applied to cells by perfusion with bathing solution. In some experiments, expression of HaloTag-fused proteins was confirmed by labeling of cells with cell-permeable HaloTag TMR ligand (Promega).

Single-particle tracking was performed with G-Count (G-Angstrom, Sendai, Japan) in a 2D Gaussian fitting mode. We tracked each particle fitted within a 13 × 13–pixel region of interest for at least 30 frames. When the signal in a frame was lost because of blinking, no fitting was performed until the bright spot reappeared; when it did not do so within 10 frames, tracking was aborted. We typically tracked 50–150 particles/cell and evaluated movements according to the MSD, which was calculated for all accessible time lags τ with the following formula:

$$\mathrm{MSD}(\tau) = \frac{1}{N - \frac{\tau}{\Delta t}} \sum_{i=1}^{N-\frac{\tau}{\Delta t}} \left| \mathbf{p}_{i+\frac{\tau}{\Delta t}} - \mathbf{p}_i \right|^2 \quad (1)$$

where N, Δt, and $\mathbf{p}_i$ are the total number of positions measured, time interval of successive images, and position of the molecule in time frame i, respectively. The diffusion coefficient (D) and velocities (v) were estimated from the MSD values by fitting with a quadratic polynomial function:

$$\mathrm{MSD}(\tau) = 4D\tau + v^2\tau^2 + C \quad (2)$$

where C is the position error. Because the MSD values would be proportional to $4D\tau$ when τ is small, instantaneous diffusion coefficients along the trajectory (Dahan *et al.*, 2003; Pinaud *et al.*, 2009) that were derived from MSD curves calculated over consecutive trajectory stretches of nine points centered around the current position

were calculated by fitting the first three points of the MSD curve to the formula

$$\mathrm{MSD}(\tau) = 4D\tau + C \quad (3)$$

In addition, MSD values typically exhibit approximate power-law behavior,

$$\mathrm{MSD}(\tau) \propto \tau^{\alpha} \quad (4)$$

and the exponent α, which can obtained as a slope of the MSD values plotted on a double-logarithmic plot, provides the characteristics of the motion: $\alpha = 0$ for an immobile particle, $\alpha = 1$ for a randomly diffusing particle, and $\alpha = 2$ for a particle showing directional movement (Nelson *et al.*, 2009). Fitting was performed by Origin. Estimated diffusion coefficients are presented as mean ± SD.

ACKNOWLEDGMENTS

We thank Fumie Wagatsuma and Natsumi Emoto for technical assistance. This work was supported in part by grants from the Japan Society for the Promotion of Science (25713010 and 26600019 to H.H. and 25293074 and 16K12863 to M.K.) and the Program for Fostering Researchers for the Next Generation in a Project for Establishing a Consortium for the Development of Human Resources in Science and Technology (to H.H.).

REFERENCES

Beach JR, Shao L, Remmert K, Li D, Betzig E, Hammer JA 3rd (2014). Nonmuscle myosin II isoforms coassemble in living cells. Curr Biol 24, 1160–1166.

Bose A, Guilherme A, Robida SI, Nicoloro SM, Zhou QL, Jiang ZY, Pomerleau DP, Czech MP (2002). Glucose transporter recycling in response to insulin is facilitated by myosin Myo1c. Nature 420, 821–824.

Bose A, Robida S, Furcinitti PS, Chawla A, Fogarty K, Corvera S, Czech MP (2004). Unconventional myosin Myo1c promotes membrane fusion in a regulated exocytic pathway. Mol Cell Biol 24, 5447–5458.

Buss F, Arden SD, Lindsay M, Luzio JP, Kendrick-Jones J (2001). Myosin VI isoform localized to clathrin-coated vesicles with a role in clathrin-mediated endocytosis. EMBO J 20, 3676–3684.

Catlett NL, Weisman LS (1998). The terminal tail region of a yeast myosin-V mediates its attachment to vacuole membranes and sites of polarized growth. Proc Natl Acad Sci USA 95, 14799–14804.

Chen FQ, Gerion D (2004). Fluorescent CdSe/ZnS nanocrystal-peptide conjugates for long-term, nontoxic imaging and nuclear targeting in living cells. Nano Lett 4, 1827–1832.

Chen XW, Leto D, Chiang SH, Wang Q, Saltiel AR (2007). Activation of RalA is required for insulin-stimulated Glut4 trafficking to the plasma membrane via the exocyst and the motor protein. Myo1c. Dev Cell 13, 391–404.

Chenouard N, Smal I, de Chaumont F, Maska M, Sbalzarini IF, Gong Y, Cardinale J, Carthel C, Coraluppi S, Winter M, *et al.* (2014). Objective comparison of particle tracking methods. Nat Methods 11, 281–289.

Chen O, Zhao J, Chauhan VP, Cui J, Wong C, Harris DK, Wei H, Han HS, Fukumura D, Jain RK, Bawendi MG (2013). Compact high-quality CdSe-CdS core-shell nanocrystals with narrow emission linewidths and suppressed blinking. Nat Mater 12, 445–451.

Choi YO, Ryu HJ, Kim HR, Song YS, Kim C, Lee W, Choe H, Leem CH, Jang YJ (2006). Implication of phosphorylation of the myosin II regulatory light chain in insulin-stimulated GLUT4 translocation in 3T3-F442A adipocytes. Exp Mol Med 38, 180–189.

Dahan M, Levi S, Luccardini C, Rostaing P, Riveau B, Triller A (2003). Diffusion dynamics of glycine receptors revealed by single-quantum dot tracking. Science 302, 442–445.

Derfus AM, Chan WCW, Bhatia SN (2004). Intracellular delivery of quantum dots for live cell labeling and organelle tracking. Adv Mater 16, 961–966.

Duan H, Nie S (2007). Cell-penetrating quantum dots based on multivalent and endosome-disrupting surface coatings. J Am Chem Soc 129, 3333–3338.

Dubertret B, Skourides P, Norris DJ, Noireaux V, Brivanlou AH, Libchaber A (2002). In vivo imaging of quantum dots encapsulated in phospholipid micelles. Science 298, 1759–1762.

Fakhri N, Wessel AD, Willms C, Pasquali M, Klopfenstein DR, MacKintosh FC, Schmidt CF (2014). High-resolution mapping of intracellular fluctuations using carbon nanotubes. Science 344, 1031–1035.

Foth BJ, Goedecke MC, Soldati D (2006). New insights into myosin evolution and classification. Proc Natl Acad Sci USA 103, 3681–3686.

Fujita H, Hatakeyama H, Watanabe TM, Sato M, Higuchi H, Kanzaki M (2010). Identification of three distinct functional sites of insulin-mediated GLUT4 trafficking in adipocytes using quantitative single molecule imaging. Mol Biol Cell 21, 2721–2731.

Fujita H, Nedachi T, Kanzaki M (2007). Accelerated de novo sarcomere assembly by electric pulse stimulation in C2C12 myotubes. Exp Cell Res 313, 1853–1865.

Fulcher FK, Smith BT, Russ M, Patel YM (2008). Dual role for myosin II in GLUT4-mediated glucose uptake in 3T3-L1 adipocytes. Exp Cell Res 314, 3264–3274.

Galland C, Ghosh Y, Steinbruck A, Hollingsworth JA, Htoon H, Klimov VI (2012). Lifetime blinking in nonblinking nanocrystal quantum dots. Nat Commun 3, 908.

Gardini L, Capitanio M, Pavone FS (2015). 3D tracking of single nanoparticles and quantum dots in living cells by out-of-focus imaging with diffraction pattern recognition. Sci Rep 5, 16088.

Giner D, Lopez I, Villanueva J, Torres V, Viniegra S, Gutierrez LM (2007). Vesicle movements are governed by the size and dynamics of F-actin cytoskeletal structures in bovine chromaffin cells. Neuroscience 146, 659–669.

Giner D, Neco P, Frances Mdel M, Lopez I, Viniegra S, Gutierrez LM (2005). Real-time dynamics of the F-actin cytoskeleton during secretion from chromaffin cells. J Cell Sci 118, 2871–2880.

Hartman MA, Spudich JA (2012). The myosin superfamily at a glance. J Cell Sci 125, 1627–1632.

Hatakeyama H, Kanzaki M (2011). Molecular basis of insulin-responsive GLUT4 trafficking systems revealed by single molecule imaging. Traffic 12, 1805–1820.

Hatakeyama H, Kanzaki M (2013a). Development of dual-color simultaneous single molecule imaging system for analyzing multiple intracellular trafficking activities. Conf Proc IEEE Eng Med Biol Soc 2013, 1418–1421.

Hatakeyama H, Kanzaki M (2013b). Regulatory mode shift of Tbc1d1 is required for acquisition of insulin-responsive GLUT4-trafficking activity. Mol Biol Cell 24, 809–817.

Hohng S, Ha T (2004). Near-complete suppression of quantum dot blinking in ambient conditions. J Am Chem Soc 126, 1324–1325.

Holtzer L, Meckel T, Schmidt T (2007). Nanometric three-dimensional tracking of individual quantum dots in cells. Appl Phys Lett 90, 053902.

Huang J, Imamura T, Olefsky JM (2001). Insulin can regulate GLUT4 internalization by signaling to Rab5 and the motor protein dynein. Proc Natl Acad Sci USA 98, 13084–13089.

Imamura T, Huang J, Usui I, Satoh H, Bever J, Olefsky JM (2003). Insulin-induced GLUT4 translocation involves protein kinase C-lambda-mediated functional coupling between Rab4 and the motor protein kinesin. Mol Cell Biol 23, 4892–4900.

Ishikura S, Klip A (2008). Muscle cells engage Rab8A and myosin Vb in insulin-dependent GLUT4 translocation. Am J Physiol Cell Physiol 295, C1016–C1025.

Ji B, Giovanelli E, Habert B, Spinicelli P, Nasilowski M, Xu X, Lequeux N, Hugonin JP, Marquier F, Greffet JJ, Dubertret B (2015). Non-blinking quantum dot with a plasmonic nanoshell resonator. Nat Nanotechnol 10, 170–175.

Kairdolf BA, Smith AM, Stokes TH, Wang MD, Young AN, Nie S (2013). Semiconductor quantum dots for bioimaging and biodiagnostic applications. Annu Rev Anal Chem 6, 143–162.

Kanzaki M, Pessin JE (2001). Insulin-stimulated GLUT4 translocation in adipocytes is dependent upon cortical actin remodeling. J Biol Chem 276, 42436–42444.

Kanzaki M, Pessin JE (2002). Caveolin-associated filamentous actin (Cav-actin) defines a novel F-actin structure in adipocytes. J Biol Chem 277, 25867–25869.

Kanzaki M, Watson RT, Khan AH, Pessin JE (2001). Insulin stimulates actin comet tails on intracellular GLUT4-containing compartments in differentiated 3T3L1 adipocytes. J Biol Chem 276, 49331–49336.

Keren K, Yam PT, Kinkhabwala A, Mogilner A, Theriot JA (2009). Intracellular fluid flow in rapidly moving cells. Nat Cell Biol 11, 1219–1224.

Kodera N, Ando T (2014). The path to visualization of walking myosin V by high-speed atomic force microscopy. Biophys Rev 6, 237–260.

Liu DS, Phipps WS, Loh KH, Howarth M, Ting AY (2012). Quantum dot targeting with lipoic acid ligase and HaloTag for single-molecule imaging on living cells. ACS Nano 6, 11080–11087.
Liu SL, Li J, Zhang ZL, Wang ZG, Tian ZQ, Wang GP, Pang DW (2013). Fast and high-accuracy localization for three-dimensional single-particle tracking. Sci Rep 3, 2462.
Los GV, Encell LP, McDougall MG, Hartzell DD, Karassina N, Zimprich C, Wood MG, Learish R, Ohana RF (2008). HaloTag: a novel protein labeling technology for cell imaging and protein analysis. ACS Chem Biol 3, 373–382.
Lowe AR, Siegel JJ, Kalab P, Siu M, Weis K, Liphardt JT (2010). Selectivity mechanism of the nuclear pore complex characterized by single cargo tracking. Nature 467, 600–603.
Mahler B, Spinicelli P, Buil S, Quelin X, Hermier JP, Dubertret B (2008). Towards non-blinking colloidal quantum dots. Nat Mater 7, 659–664.
Mathur J, Mathur N, Kirik V, Kernebeck B, Srinivas BP, Hulskamp M (2003). Arabidopsis CROOKED encodes for the smallest subunit of the ARP2/3 complex and controls cell shape by region specific fine F-actin formation. Development 130, 3137–3146.
Miserey-Lenkei S, Chalancon G, Bardin S, Formstecher E, Goud B, Echard A (2010). Rab and actomyosin-dependent fission of transport vesicles at the Golgi complex. Nat Cell Biol 12, 645–654.
Nelson SR, Ali MY, Trybus KM, Warshaw DM (2009). Random walk of processive, quantum dot-labeled myosin Va molecules within the actin cortex of COS-7 cells. Biophys J 97, 509–518.
Odronitz F, Kollmar M (2007). Drawing the tree of eukaryotic life based on the analysis of 2,269 manually annotated myosins from 328 species. Genome Biol 8, R196.
Peck GR, Chavez JA, Roach WG, Budnik BA, Lane WS, Karlsson HK, Zierath JR, Lienhard GE (2009). Insulin-stimulated phosphorylation of the Rab GTPase-activating protein TBC1D1 regulates GLUT4 translocation. J Biol Chem 284, 30016–30023.
Pierobon P, Achouri S, Courty S, Dunn AR, Spudich JA, Dahan M, Cappello G (2009). Velocity, processivity, and individual steps of single myosin V molecules in live cells. Biophys J 96, 4268–4275.
Pierobon P, Cappello G (2012). Quantum dots to tail single bio-molecules inside living cells. Adv Drug Deliv Rev 64, 167–178.
Pinaud F, Michalet X, Iyer G, Margeat E, Moore HP, Weiss S (2009). Dynamic partitioning of a glycosyl-phosphatidylinositol-anchored protein in glycosphingolipid-rich microdomains imaged by single-quantum dot tracking. Traffic 10, 691–712.
Riedl J, Crevenna AH, Kessenbrock K, Yu JH, Neukirchen D, Bista M, Bradke F, Jenne D, Holak TA, Werb Z, *et al*. (2008). Lifeact: a versatile marker to visualize F-actin. Nat Methods 5, 605–607.
Ruthardt N, Lamb DC, Brauchle C (2011). Single-particle tracking as a quantitative microscopy-based approach to unravel cell entry mechanisms of viruses and pharmaceutical nanoparticles. Mol Ther 19, 1199–1211.
Sandquist JC, Means AR (2008). The C-terminal tail region of nonmuscle myosin II directs isoform-specific distribution in migrating cells. Mol Biol Cell 19, 5156–5167.
Sano H, Kane S, Sano E, Miinea CP, Asara JM, Lane WS, Garner CW, Lienhard GE (2003). Insulin-stimulated phosphorylation of a Rab GTPase-activating protein regulates GLUT4 translocation. J Biol Chem 278, 14599–14602.
Saxton MJ (2008). Single-particle tracking: connecting the dots. Nat Methods 5, 671–672.
Seabra MC, Coudrier E (2004). Rab GTPases and myosin motors in organelle motility. Traffic 5, 393–399.
Semiz S, Park JG, Nicoloro SM, Furcinitti P, Zhang C, Chawla A, Leszyk J, Czech MP (2003). Conventional kinesin KIF5B mediates insulin-stimulated GLUT4 movements on microtubules. EMBO J 22, 2387–2399.
Snyder GE, Sakamoto T, Hammer JA, Sellers JR, Selvin PR (2004). Nanometer localization of single green fluorescent proteins: evidence that myosin V walks hand-over-hand via telemark configuration. Biophys J 87, 1776–1783.
So MK, Xu C, Loening AM, Gambhir SS, Rao J (2006). Self-illuminating quantum dot conjugates for in vivo imaging. Nat Biotechnol 24, 339–343.
So MK, Yao H, Rao J (2008). HaloTag protein-mediated specific labeling of living cells with quantum dots. Biochem Biophys Res Commun 374, 419–423.
Steimle PA, Fulcher FK, Patel YM (2005). A novel role for myosin II in insulin-stimulated glucose uptake in 3T3-L1 adipocytes. Biochem Biophys Res Commun 331, 1560–1565.
Sun C, Cao Z, Wu M, Lu C (2014). Intracellular tracking of single native molecules with electroporation-delivered quantum dots. Anal Chem 86, 11403–11409.
Suzuki Y, Roy CN, Promjunyakul W, Hatakeyama H, Gonda K, Imamura J, Vasudevanpillai B, Ohuchi N, Kanzaki M, Higuchi H, Kaku M (2013). Single quantum dot tracking reveals that an individual multivalent HIV-1 Tat protein transduction domain can activate machinery for lateral transport and endocytosis. Mol Cell Biol 33, 3036–3049.
Thompson MA, Lew MD, Badieirostami M, Moerner WE (2010). Localizing and tracking single nanoscale emitters in three dimensions with high spatiotemporal resolution using a double-helix point spread function. Nano Lett 10, 211–218.
Tsakraklides V, Krogh K, Wang L, Bizario JC, Larson RE, Espreafico EM, Wolenski JS (1999). Subcellular localization of GFP-myosin-V in live mouse melanocytes. J Cell Sci 112, 2853–2865.
Vicente-Manzanares M, Zareno J, Whitmore L, Choi CK, Horwitz AF (2007). Regulation of protrusion, adhesion dynamics, and polarity by myosins IIA and IIB in migrating cells. J Cell Biol 176, 573–580.
Watanabe TM, Fujii F, Jin T, Umemoto E, Miyasaka M, Fujita H, Yanagida T (2013). Four-dimensional spatial nanometry of single particles in living cells using polarized quantum rods. Biophys J 105, 555–564.
Watanabe T, Hosoya H, Yonemura S (2007a). Regulation of myosin II dynamics by phosphorylation and dephosphorylation of its light chain in epithelial cells. Mol Biol Cell 18, 605–616.
Watanabe TM, Sato T, Gonda K, Higuchi H (2007b). Three-dimensional nanometry of vesicle transport in living cells using dual-focus imaging optics. Biochem Biophys Res Commun 359, 1–7.
Yip MF, Ramm G, Larance M, Hoehn KL, Wagner MC, Guilhaus M, James DE (2008). CaMKII-mediated phosphorylation of the myosin motor Myo1c is required for insulin-stimulated GLUT4 translocation in adipocytes. Cell Metab 8, 384–398.
Yoshizaki T, Imamura T, Babendure JL, Lu JC, Sonoda N, Olefsky JM (2007). Myosin 5a is an insulin-stimulated Akt2 (protein kinase Bbeta) substrate modulating GLUT4 vesicle translocation. Mol Cell Biol 27, 5172–5183.